Overcoming photodamage in second-harmonic generation microscopy: Real-time optical recording of neuronal action potentials

L. Sacconi*†, D. A. Dombeck*, and W. W. Webb*‡

*School of Applied and Engineering Physics, Cornell University, Ithaca, NY 14853; and †European Laboratory for Nonlinear Spectroscopy, University of Florence, 50019 Sesto Fiorentino, Italy

Contributed by W. W. Webb, December 31, 2005

Second-harmonic generation (SHG) has proven essential for the highest-resolution optical recording of membrane potential (Vm) in intact specimens. Here, we demonstrate single-trial SHG recordings of neuronal somatic action potentials and quantitative recordings of their decay with averaging at multiple sites during propagation along branched neurites at distances up to 350 μm from the soma. We realized these advances by quantifying, analyzing, and thereby minimizing the dynamics of photodamage (PD), a frequent limiting factor in the optical imaging of biological preparations. The optical signal and the PD during SHG imaging of stained cultured *Aplysia* neurons were examined with intracellular electrode recordings monitoring the resting Vm variations induced by laser-scanning illumination. We found that the PD increased linearly with the dye concentration but grew with the cube of illumination intensity, leading to unanticipated optimization procedures to minimize PD. The addition of appropriate antioxidants in conjunction with an observed Vm recovery after termination of laser scanning further refined the imaging criteria for minimization and control of PD during SHG recording of action potentials. With these advances, the potential of SHG as an effective optical tool for neuroscience investigations is being realized.

voltage imaging | membrane potential | neural imaging | *Aplysia*

The optical recording of membrane potential (Vm) provides a powerful tool for investigating the mechanisms of rapid signal transduction in the nervous system (1, 2). In contrast with electrode methods, optical techniques provide the ability to measure Vm simultaneously from many neurons in a network and/or from many positions on one neuron. This capability is crucial for the study of intact neural systems (3) and their interconnections that may be too small or fragile for electrode recordings (4, 5).

Recently, second-harmonic generation (SHG) microscopy has been developed for the optical recording of Vm in living cells with high spatio-temporal resolution ($\approx$1 μm and $\approx$1 ms) (6, 7). An important advantage of SHG for Vm recording is that the signal emanates only from properly ordered dye molecules in the plasma membrane, whereas randomly oriented dye molecules bound to nearby intracellular or extracellular components do not contribute to the SHG signal (8, 9). Therefore, the signal response to Vm is not degraded by background, as it is for fluorescence (7, 10). Furthermore, the signal response to Vm is linear (as with fluorescence) (11, 12), providing SHG with the ability to relate directly the signal responses to changes in Vm. Because SHG is a nonlinear optical phenomenon, it maintains the deep-tissue, high-resolution imaging advantages of two-photon fluorescence (TPF) microscopy (13–15). These advantages over conventional fluorescence methods make SHG microscopy the technique of choice for high-resolution Vm recording deep in tissue slice preparations and presumably also *in vivo* (7).

On the other hand, biological application of Vm measurements with SHG microscopy (and fluorescence methods) are usually signal-to-noise (S/N) limited by photodamage (PD). Because the SHG signal voltage responses are small, high illumination intensity and/or high dye concentration are needed to attain useful S/N. Dombeck *et al.* (6, 7) increased S/N by temporal averaging of consecutive line scans, which made it possible to optically record action potentials (APs) on soma and neurite membranes of neurons in culture and brain slice. Nevertheless, this method did not allow the recording of electrophysiological events in a single trial with useful S/N. Consequently, the investigation of many outstanding problems in electrophysiology, neurobiology, and biomedical diagnostics still appeared inaccessible.

Because PD reduction has been successfully implemented for some linear optical Vm detection methods to increase S/N (16, 17), we also explored the possibility of PD reduction to enhance the technique of optical Vm recording with SHG. In this research, the signal and PD of SHG imaging of cultured *Aplysia* neurons loaded with FM4-64 dye were examined. We used FM4-64 dye because it currently appears to be the most promising SHG probe for fast optical recording of Vm in intact preparations (7, §). Because these recordings probe the electrophysiological state of the system, the quantification of the resting Vm should provide the most relevant real-time indicator of the PD. For this reason, we used intracellular electrode recordings to monitor laser illumination-induced changes in the neuronal resting Vm. This methodology enabled the quantification of PD evolution in various scanning configurations; specifically, we investigated the reduction of the resting Vm versus excitation laser power and dye concentration in line- and image-scanning configurations. The recovery of the resting Vm to preillumination levels after termination of scanning was investigated. We also studied the PD process in anaerobic conditions and in the presence of various antioxidants. The understanding of PD attained through these studies was applied to increase the S/N of optical SHG recording of APs. Thus we report major advances of SHG recording of APs at the soma in a single trial and the quantification of the AP amplitude with averaging at many neurite positions extending to distances up to 350 μm from the soma.

Results

SHG Sensitivity and S/N Measurements. The SHG Vm sensitivity and S/N in FM4-64-stained *Aplysia* neurons were measured by

Conflict of interest statement: No conflicts declared.

Freely available online through the PNAS open access option.

Abbreviations: PD, photodamage; SHG, second-harmonic generation; Vm, membrane potential; AP, action potential; TPF, two-photon fluorescence; S/N, signal-to-noise; dc, duty cycle.

‡To whom correspondence should be addressed. E-mail: www2@cornell.edu.

§Yuste, R., Nemet, B., Jiang, J., Nuriya, M. & Eisenthal, K., Imaging Neurons and Neural Activity: New Methods Meeting, March 10–13, 2005, Cold Spring Harbor, NY, abstr. 16.

© 2006 by The National Academy of Sciences of the USA

www.pnas.org/cgi/doi/10.1073/pnas.0511338103

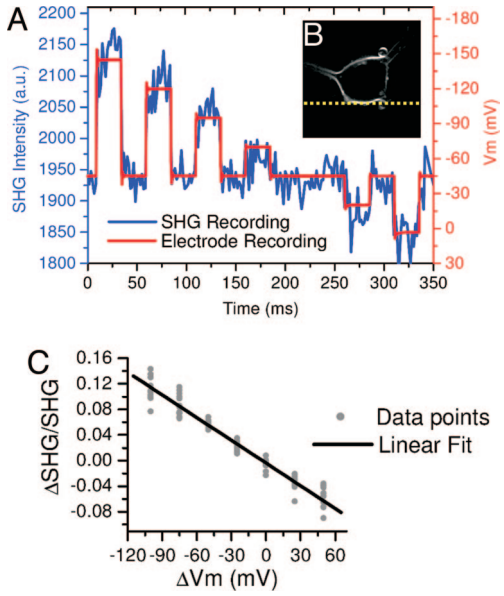

Fig. 1. Line-scan recording of Vm with SHG in cultured *Aplysia* neurons. (*A*) The blue trace obtained with temporal averaging of 20 consecutive scans shows the intensity plot of SHG emission [in arbitrary units (a.u.), left-axis scale] versus time. SHG signal changes were recorded by line scanning and averaging all membrane pixels across the line denoted in *B* (600 lines per s). The voltage-clamped neuron was given 35-ms duration ΔVm steps. The red trace represents the electrode Vm measurement (right-axis scale). (*B*) A single SHG *z*-section through an *Aplysia* neuron stained with FM4-64 (image: 100 × 100 μm). The dashed yellow line represents the scanned line. (*C*) Plot of ΔSHG/SHG over physiologically relevant ΔVm (red trace in *A*; $n = 8$ cells used). The functional fit in black shows a linear relationship ($R^2 = 0.995$).

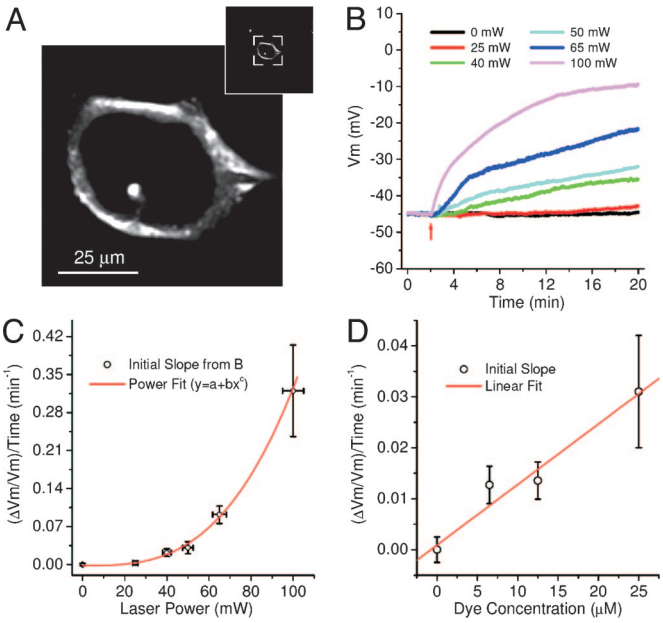

Fig. 2. PD in image-scanning mode. (*A*) A single TPF *z*-section through an *Aplysia* neuron stained with FM4-64. The dye is easily internalized by the cell, labeling the cytoplasm and the plasma membrane. (*Inset*) Actual zoom used during PD experiments. (*B*) Resting Vm traces during irradiation (irradiation start at red arrow) with various laser powers to show decrease of Vm caused by PD during excessive exposure (dye concentration 25 μM). Each trace represents the mean of a set of 45-mV Vm-normalized traces ($n = 6$–10 for each laser power). (*C*) Dependence of the relative initial variation rates of Vm caused by PD (initial slope) on the laser power (from the traces in *B*). The data points (open circles) were fitted with a power-law function (red line, $\chi^2 = 0.39$). See text for best-fit parameters. (*D*) Dependence of the relative rates of initial variation of Vm caused by PD on the dye concentration (laser power 50 mW). The red line represents the best linear fit ($R^2 = 0.90$).

using fast voltage steps applied to the voltage-clamped cells (Fig. 1*A*). The necessary temporal resolution to optically detect fast neuronal Vm transients with SHG was obtained by using the line-scanning mode (1,200 lines per s with 256 pixel per line and no SHG signal collection during focal spot fly-back). The line scans were oriented parallel to the soma membrane (Fig. 1*B*) to increase the S/N (7). The line-scanning and voltage steps were synchronized through trigger pulses coupling the amplifier and image acquisition software. Fig. 1*A* shows the average of 20 SHG line scans, with 4 s between consecutive scans, 12-mW laser power, and 25-μM dye concentration. Vm-induced SHG signal changes in eight different cells are plotted in Fig. 1*C*, which shows a linear response of the SHG with respect to ΔVm [$\Delta SHG/SHG = -(11.8 \pm 0.4)\cdot10^{-4}\ \Delta Vm/mV$], in agreement with previous results (7). A Vm step of −100 mV leads to a S/N ≈1 for a single trace that collects photons for ≈5 μs per membrane pass, necessitating temporal averaging. The modulations of the SHG emission followed the applied voltage steps, with S/N ≈4–6, after averaging 20 line scans (Fig. 1*A*). With this laser power and dye concentration we were able to collect ≈2 SHG photons per μs while scanning on the membrane.

PD Measurements in Image-Scanning Mode. Next, we investigated variations of the resting Vm caused by PD in neurons subjected to laser illumination. Microelectrode recordings were used to record the resting Vm for 20 min. The resting Vm in unstained and nonilluminated samples is stable, with negligible temporal fluctuation <0.14 mV per min, with values ranging from −25 to −70 mV (average of 10 cells: −45.6 ± 5.0 mV). To study the effect of the laser irradiation, we continuously imaged the same optical section of stained neuronal somas with the following parameters: image resolution, 512 × 512 pixels; image dimension, ≈200 × 200 μm; 1,000 lines per s (no fly-back collection or blanking). In the absence of other optical processes, SHG cannot cause PD because the underlying HyperRayleigh scattering process involves no molecular energy absorption. However, in the best-known Vm probes, SHG is always accompanied by TPF (7), where thermal and photochemical excited-state processes leading to PD occur. Fig. 2*A* shows a TPF image of an *Aplysia* neuron soma. It shows that FM4-64 can easily be internalized by the cell and, in principle, the harmful photoproducts could harm the plasma membrane or intracellular organelles. However, we expect that during the time of our measurements (in some cases only seconds for signs of damage to be seen) the variation of the resting Vm is caused mostly by direct plasma membrane damage (see *Discussion and Conclusions*). Considering the *Aplysia* soma diameter (40–60 μm) and the radial dimension of the excitation focal volume (≈1 μm), we find that the time that the focal volume scans over the membrane in image-scanning mode is ≈5 ms per scan, leading to a duty cycle (dc) of ≈0.25% ($dc = t_{il}/t_s$, where t_{il} is the time that the focal volume illuminates the membrane and t_s is the scan time for a full image). Fig. 2*B* shows the variation of the Vm during irradiation with various laser powers, but fixed staining concentration (25 μM). The cells were irradiated just after the first 2 min of Vm acquisition (red arrow in Fig. 2*B*). Fig. 2*C* shows the dependence of the initial relative rate of change of Vm caused by PD, computed from the initial slope of the traces of damage shown in Fig. 2*B*, on the laser power. By fitting the data points with a power function ($y = a + bx^c$) we obtain the following best-fit values: $a = (-0.0019 \pm 0.034)\ min^{-1}$, $b = (3.1 \pm 4.7)\cdot10^{-7}\ min^{-1}\cdot(mW)^{-c}$, and $c = 3.01 \pm 0.35$. The small a value indicates that labeling of the membrane with FM4-64 does not

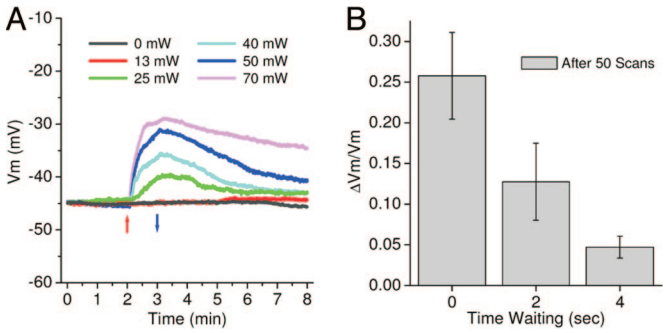

Fig. 3. PD in line-scanning mode. (*A*) Shown are six traces of the resting Vm during and after the 1-min irradiation [red (up) and blue (down) arrows mark the start and the end of line scan, respectively] with various laser powers (dye concentration 25 μM). Each trace represents the mean of a set of 45-mV Vm-normalized traces. Note that the Vm recovers after the termination of laser irradiation and that the line-scan PD is larger than the image-scan PD in Fig. 2*B*. Using a single exponential decay fit, we find characteristic recovery times of 5 and 1–2 min after the irradiation with high (70–50 mW) and low powers (40–25 mW), respectively. (*B*) Relative variation of Vm after 50 consecutive line scans (dye concentration 25 μM, laser power 50 mW) versus the waiting time between individual scans (n = 6 cells for each waiting time).

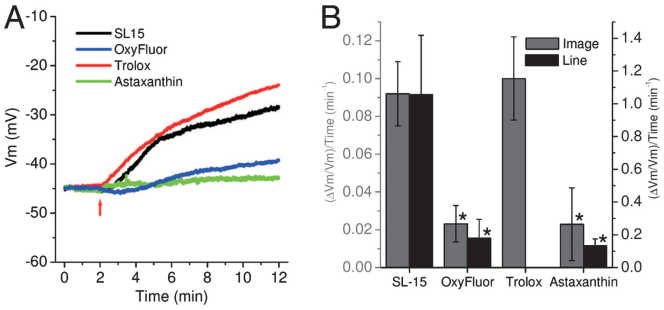

Fig. 4. PD reduction by application of antioxidants or anaerobic conditions. (*A*) Vm damage recordings in the absence (SL-15) or the presence of an oxygen-reducing agent (OxyFluor) or two different antioxidants (Trolox and Astaxanthin). The four traces show the behavior of the resting Vm during the irradiation in image-scan mode (dye concentration 25 μM). (*B*) Comparison of the relative initial variation rates of Vm caused by PD in the absence and presence of OxyFluor or antioxidants in image (gray bars, left-axis scale) or line (dark gray bars, right-axis scale) scanning modes (n = 5–7 for each case). The laser powers were 65 and 50 mW for image and line scan, respectively. Statistically significant reduction of the cell damage was determined by a t test (*, $P < 0.05$).

induce any pharmacological effects. The cubic exponent shows a highly nonlinear dependence of the PD on the laser power. In this laser-power range (from 25 to 100 mW) the TPF (and SHG) signal strength is near saturation [signal is linear with respect to laser power ($R^2 = 0.999$)], whereas a quadratic (2.10 ± 0.09) TPF signal (and SHG) dependence was observed for lower powers (from 0.1 to 5 mW) (data not shown). The implications and the possible physical origins of these observations are discussed below. Although by our definition the b coefficient is independent of excitation power, it depends on many other experimental parameters (dc, excitation wavelength, dye concentration, oxygen concentration, objective numerical aperture, cell compartment, etc.) that can alter the PD.

Using the same methods, we also investigated the PD dependence on dye concentration. Fig. 2*D* shows the relative Vm variation velocity dependence on the dye concentration, with a fixed laser power (50 mW). By fitting the data points with a linear function ($y = n + mx$) we obtained $n = (9 \pm 22)\cdot 10^{-4}$ min^{-1} and $m = (0.0012 \pm 0.0003)$ (min$\cdot\mu$M)$^{-1}$ with $R^2 = 0.90$. The n value indicates that the PD is caused entirely by laser illumination of the dye, whereas the linear relationship between PD and dye concentration points to a linear proportionality between the b coefficient above and the dye concentration.

PD Measurements in Line-Scanning Mode. Using the same methods, we investigated the variation of the resting Vm caused by PD in line-scanning mode. Continuous line scanning (1,000 lines per s, no fly-back collection or blanking, 512 pixels per line) was performed normal to the soma membrane to ensure a similar illuminated area for all trials. Fig. 3*A* shows the variation of the resting Vm during and after irradiation with various levels of laser power. The line scans were started after 2 min of Vm recording (red arrow in Fig. 3*A*) and stopped after 1 min of irradiation (blue arrow in Fig. 3*A*). The neurons (n = 7–8 for each laser power) were stained with a 25-μM dye concentration. By fitting the initial slopes with a power function (as above) we obtained the following best-fit parameters: $a = (-0.022 \pm 0.006)$ min^{-1}, $b = (2 \pm 2)\cdot 10^{-5}$ min$^{-1}\cdot$(mW)$^{-c}$, and $c = 2.76 \pm 0.20$. For this fitting, the data point at 70 mW was removed because of suspected PD saturation. These results confirm the highly nonlinear dependence of the PD on the laser power found in the image-scanning mode. The b parameter is much larger than in the image-scan mode. This result can be partly associated with the increased dc of line scan mode (≈1.2%) versus image scan mode (≈0.25%). Because PD is likely to be linearly related to the illumination time (without considering saturation effects, Figs. 2*B* and 3*A*), this factor of five difference in the dc (and hence the illumination time) cannot account for the two orders of magnitude difference in b. The other major difference between line and image scanning is the time that is allowed between successive illuminations of the same membrane position, allowing for differences in any membrane recovery that may occur. Because this time is drastically reduced in line versus image scanning, it may account for the large difference in b coefficients. Fig. 3*A* shows this likely possibility; after the termination of line scanning the neuronal Vm can recover to preillumination levels. To further investigate the implication that the recovery time may strongly affect the damage, we studied the dependence of the PD on the time between each consecutive line scan in a practical configuration. Following a methodology similar to Dombeck *et al.* (6, 7), we irradiated the sample with 500 lines per individual line scan (scanning rate of 1,000 lines per s) for 50 scans. In this experiment the laser power and dye concentration were fixed at 50 mW and 25 μM, respectively, but the waiting time between each individual line scan was varied from 0 to 4 s. Over this range a large reduction of the PD with increased waiting time was observed (Fig. 3*B*). In comparison to the continuous line-scan configuration (time wait 0 s) we found damage reductions of factors of ≈2 and ≈5 with waiting times of 2 and 4 s, respectively.

PD Dependence on Oxygen. Using an oxygen scavenging enzyme (OxyFluor, Oxyrase, Mansfield, OH), we measured the significant role of oxygen in the PD process in both image- and line-scanning modes. Fig. 4 shows a comparison between irradiated neurons under aerobic or anaerobic conditions. For each scanning configuration a large reduction of the PD in anaerobic conditions was observed. In particular, Fig. 4*B* shows damage reduction by a factor ≈5. This damage reduction result suggests that the photochemical production of singlet oxygen by FM4-64 is likely to be the predominant source of PD. To extend this result to applications in aerobic biological systems (i.e., mammalian brain slices) we studied the PD in the presence of two potent antioxidants, Trolox (Sigma) (19) and Astaxanthin (Sigma) (20). By using the image-scanning configuration we found that with or without Trolox (1 mM) the laser irradiation produced statistically identical damage (Fig. 4). Increasing the Trolox concentration from 1 to 10 mM resulted in significant changes in the

electrophysiological behavior of the neurons. Because of the low membrane partitioning coefficient of the Trolox, only a small amount of the antioxidant is present within the membrane to limit damage from singlet oxygen, thus this negative result with Trolox is not surprising. On the other hand, Astaxanthin is an extremely hydrophobic antioxidant with a high membrane partitioning coefficient (21). In fact, the presence of this reactive oxygen-scavenging species produces a large reduction in the damage (for both image- and line-scanning modes) statistically comparable to anaerobic conditions (Fig. 4). Furthermore, no electrophysiological alterations were observed.

Determination of Single-Trial SHG AP Recording Parameters. Here we apply the knowledge from the PD studies of the previous sections to optimize the optical recording of APs. From these PD studies we found a linear relationship between the PD rate and dye concentration, but a third-order relation between the PD rate and the illumination intensity. These results, in combination with the fact that SHG intensity scales with the square of the number of molecules (22) (experimentally verified in our system), and that the SHG signal emission saturates with laser powers >10 mW, indicated that it is more beneficial to increase the dye concentration rather than the laser power. Furthermore, with laser powers >50 mW we observed a drastic increase in photobleaching (exponential temporal reduction of the SHG photon flux), setting an upper limit on the power. Following these considerations, the SHG photon flux was increased by saturating the plasma membrane by applying 50 μM of dye and using a laser power of 50 mW. From the SHG photon flux results, the staining saturation, and the fact that at these high laser powers the SHG signal had become linear in the excitation power (see above), we estimated ≈8 SHG photons per μs while scanning on the membrane with these parameters. Furthermore, considering the photobleaching at this power, only 150 lines per scan (1,200 lines per s; with fly-back collection, 256 pixels per line) were possible. To achieve a S/N capable of discriminating a ≈100-mV AP (S/N ≈4) in a single trial, it is necessary to orient the line scan parallel to the membrane with an appropriate zoom factor to allow for an ≈130-μs signal integration time per membrane pass. If we extrapolate the line-scanning mode damage studies to this longer integration time (increased dc), we can estimate that such a recording is possible with ≈1% Vm change per 150 scanned lines in a single-trial recording. The recovery time for each membrane position in the line-scanning configuration is likely independent of dc, therefore any increase in damage should only stem from the increased illumination time (increased dc).

Recording of APs in a Single Trial. Using the optima deduced above to set our experimental parameters, we were able to record APs in a single trial by using SHG (Fig. 5*A*). As shown in Fig. 5*A*, the S/N (≈3–5) is sufficient to clearly discriminate the APs above the noise. To obtain a more quantitative optical measure of the AP amplitude, we increased the S/N (to ≈10–15) with temporal averaging of 10 consecutive line scans (Fig. 5*B*). Specifically, we measured an amplitude of 120 ± 20 mV optically with SHG versus 100 mV measured by the microelectrode (Fig. 5*C*). For averaging, we exploited the PD study results by using a waiting time between each individual line scan of 4 s. These imaging parameters did not cause a significant variation of the resting potential or AP shape, duration, or amplitude between the first and last line scans (Fig. 5*C*) [n = 8 different cells, many showing APs with undershoots (23)]. Although the use of protective antioxidants was not needed at these high laser powers because photobleaching became the power-limiting factor, understanding the relevant PD parameters has clearly allowed for increased S/N optical recording of APs on the soma in aerobic conditions. Although these scanning parameters used at the soma can induce damage in the neurites, we were able to apply the knowledge from our antioxidant studies to quantitatively record APs along neurites.

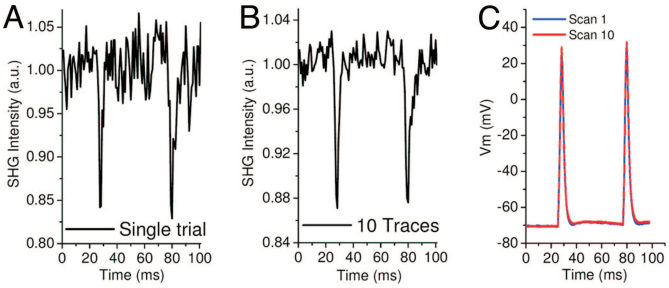

Fig. 5. Single-trial SHG recording of APs. (*A*) Normalized intensity plot of SHG emission versus time at 1,200 lines per s (0.833 ms per line) obtained from a single line scan on a neuron soma. Two APs were elicited by current injection, one at 25 ms and the other at 77 ms (blue trace in *C*), during the line scan. (*B*) SHG trace obtained by the temporal averaging of 10 line scans (waiting time between each line scan 4 s). (*C*) Microelectrode Vm recordings at the soma during the first (scan 1, blue line) and last (scan 10, red line) line scan.

SHG Recording of APs Along Neuron Neurites. The quantification of neurite PD is difficult because the damage is highly variable from neurite to neurite; consequently, a quantitative analysis is elusive. However, we did find that the neurites are more susceptible to PD than the soma, a reduction in laser power by a factor of ≈2 was needed, similar to previous results (6, 7). Furthermore, we observed that repetitive measurements using the scanning guidelines of the last section can eventually induce neurite morphological changes and variations of the resting potential and AP profile. On the other hand, by using Astaxanthin as an antioxidative protector we were able to perform sufficient repetitive SHG recordings of APs along neurites without any detectable PD, even using 50 mW of excitation power and 130 μs of integration time. Fig. 6 shows the optical recording of APs at several positions along a neurite, with some positions >350 μm distal from the somatic elicitation site. SHG recordings at each position were performed by temporal averaging of 20 line scans using a 4-s waiting time between line scans. In comparison

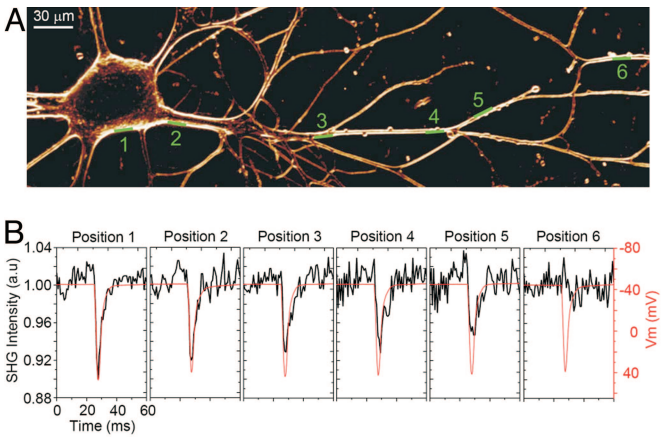

Fig. 6. SHG recording of APs along neuron neurite. (*A*) SHG projection image of 15 1-μm-thick *z*-sections through an *Aplysia* neuron stained with FM4-64. The green lines indicate the position for each line scan during the SHG recording of APs. The retractile neurite between positions 5 and 6 is typical of cultured *Aplysia* neurons and was not caused by laser illumination. (*B*) The black traces (left-axis scale), obtained from the averaged line scans, are normalized intensity plots of SHG emission versus time at the membrane positions shown in *A*. The red traces (right-axis scale) are the Vm from the recording electrode at the soma.

to somatic recordings we increased the number of trials to compensate for the reduced SHG signal emanating from the neurites. This reduction is probably associated with geometrical differences between the membrane curvatures and, consequently, a difference in the number of dye molecules oriented to be excited along the optical beam polarization direction.

It was possible to quantify the AP amplitude at many different positions over neurons by averaging 20 line scans at each position (Fig. 6). Fig. 6*B* shows a progressive attenuation of the neurite AP amplitude with increasing distance from the soma (black traces in Fig. 6*B*), whereas the microelectrode-recorded somatic AP profile remains constant (red traces in Fig. 6*B*). Fig. 6*B* is an example of recordings that suggest passive conduction of APs along neurites (24, 25). On the other hand, examples of active propagation, with AP amplitude measured by SHG to remain similar at the soma and neurite positions up to 400 μm distal from the somatic elicitation site were seen in neurites of other cells (data not shown).

Discussion and Conclusions

The capabilities of nonlinear optical imaging of biological systems continue to advance (14, 15). In particular, SHG displays suitable capabilities for important applications in the life sciences (26–30). SHG optical recording of Vm in living cells with high spatio-temporal resolution offers outstanding potential. Presently, the S/N for Vm imaging (and other microscopy applications) is usually limited by PD. Although multiphoton excitation limits PD to the focal plane, the possibility of prohibitive damage there remains as a consideration.

Damage induced during irradiation by fs laser pulses has been studied by using various criteria by Konig *et al.* (31–33). Koester *et al.* (34) and Hopt and Neher (35) studied the damage during fluorescent calcium imaging; they reported high-order (>2) PD versus illumination intensity. In our research, the variation of the resting Vm reflects the PD to FM4-64-stained cells during laser illumination. In particular, we found a highly nonlinear (third order) relation between the damage and the illumination intensity, but a linear relationship between the PD and dye concentration. Furthermore, reducing the bath oxygen potential greatly reduced the PD, implicating photochemical production of singlet oxygen by FM4-64 as the predominant source of damage in our system. From these results we can speculate on a PD scheme where the interaction between the pulsed laser light, dye molecules, and oxygen produces singlet oxygen, by some third-order photochemical process. Then, by a nearly linear biochemical process (see the relationship between the PD and dye concentration), the interaction between the singlet oxygen and neuron membrane (both lipid molecules and embedded proteins) reduces the resting Vm. This reduction is likely caused by an increase in the membrane permeability, evidenced by a decrease in cell input resistance (data not shown).

The photochemical production of singlet oxygen requires an intersystem crossing that, by a spin flip, populates the lowest-energy triplet state of the dye molecule. It is interesting to observe that higher-order photobleaching (also linked to a singlet to triplet-state transition) rates have also been suggested (36–38). Such observations suggest that a mixture of higher-order photon interactions can occur during the triplet-state population process. Following this consideration, our results may be explained by three-photon interactions (39) during this population process, perhaps associated with three-photon excitation of FM4-64 via its known small UV absorption peak, or by more complicated photodynamic processes reported by Mertz (40). On the other hand, Neuman *et al.* (41), during the characterization of one-photon PD to *Escherichia coli* in optical traps, found a linear relationship between the cell damage and the illumination intensity. This observation can be associated with a linear photochemical production of singlet oxygen during the one-photon process. If we hypothesize that the specific chromophore present does not drastically change the relationship between illumination intensity and PD in one-photon and multiphoton processes, then these results suggest that the major S/N limitation of nonlinear microscopy, with respect to conventional one-photon techniques, is PD. However, at the moment, nonlinear microscopy is the only optical technique capable of deep-tissue imaging with high resolution, making PD characterization and its possible reduction through the use of antioxidants indispensable.

As with previous studies (17) we found that the high membrane partitioning coefficient of Astaxanthin is necessary to aid in its remarkably effective PD reduction. This result adds credence to our hypothesis that the variation of the resting Vm during laser illumination is largely caused by direct membrane or membrane-embedded protein damage. Furthermore, Astaxanthin produces a large reduction of the PD statistically comparable to anaerobic conditions, implying that it provides near-total reduction of harmful photo products, here presumably singlet oxygen.

The dynamic quantification of cell damage has allowed us to observe that the resting Vm can recover after laser illumination. Comparing the characteristic 1- to 5-min recovery time to the $\approx$0.5-μs lifetime of the singlet oxygen we can speculate that the resting Vm recovery is caused by membrane or membrane protein repair. Our methodology and results concerning the dynamic quantification of PD seem likely to be applicable to many dye indicators and biological systems. In particular, future studies should attempt to characterize the possible PD reduction by Astaxanthin in intact mammalian brain tissue; however, delivery to membranes in tissue is a major problem to overcome with this and other potent, hydrophobic antioxidants such as betacarotene and lycopene.

We have applied the results of our PD studies to increase the S/N of optical recording of APs with SHG. We reported SHG recording of APs in a single trial at the soma and SHG AP amplitude quantification with averaging at many distal neurite positions. The SHG recording of APs in a single trial should prove useful for real-time investigations of neural activity deep in living networks. The imaging guidelines used for maximizing the S/N in single-trial experiments are constrained by photobleaching (and consequently by the S/N). For this reason, it is hoped that the design of new SHG probes will soon lead to increased SHG sensitivity but also reduced photobleaching compared with FM4-64. The high membrane contrast and linear response of SHG to ΔVm provide the advantage that signal changes are not degraded by background and can be directly quantified in terms of ΔVm. By temporal averaging of consecutive line scans we have exploited this phenomenon to quantify AP amplitudes in the cell soma and along neurites. In particular, we reported a progressive attenuation of AP amplitude at many positions along some neuron neurites and no attenuation along other neuron neurites; such measurements are currently difficult or inaccessible with fluorescence techniques. These recordings should be useful for a wide variety of neurophysiology applications including the testing of mathematical and computational models of AP propagation.

Materials and Methods

Imaging. The basic design of our imaging system has been described (6, 7, 28). Briefly, a 1,064 $\pm$ 15-nm fiber laser (FEMTOPOWER 1060, Fianium, Eugene, OR) with $\approx$300-fs pulses (measured at the laser output by an autocorrelator) at 70 MHz was coupled to the scanning system (Radiance 2000, Bio-Rad). A physiology objective ($\times$40, 0.8 numerical aperture) was used for epi-collection of TPF, a 0.8 numerical aperture condenser for collection of the transmitted SHG signal, 530/30-nm and 580/150-nm optical filters for SHG and TPF detection, respectively, and GaAsP photomultipliers (H7422, Hamamatsu, Middlesex, NJ) for signal detection. Pockels cell focal spot fly-back blanking was not used. The excitation laser

power was measured after the objective (at the sample) by a thermal head laser power meter (POWER MAX 5200, Molectron, Santa Clara, CA).

Microelectrode Recording. *Aplysia* neuron electrophysiological recordings were made at room temperature with an amplifier (Axoclamp 2B, Axon Instruments, Union City, CA) and PCLAMP 8.1 software (Axon Instruments). Sharp electrodes (8–15 MΩ, filled with 3 M KCl) were used to record the Vm. A two-electrode voltage clamp was used to clamp the Vm at defined values. For AP stimulation, we used two microelectrodes, one for Vm recording and one for elicitation via current injection. Temporally reproducible APs were stimulated with short, intense current pulses (30–100 nA, 1.0- to 3.5-msec duration) as in ref. 6. Each electrophysiology record was performed after the stabilization of the resting Vm (5–15 min after the microelectrode break-in).

Cell Preparation and Staining. *Aplysia* neuron cultures were prepared as in ref. 6. For dye staining, the culture solution [50% SL-15 medium (42) and 50% Hemolymph] was replaced with SL-15 containing FM4-64 dye (T3166, Molecular Probes), and 0.22 μm was filtered and incubated for $\approx$1 min. The sample was then mounted on the microscope for microelectrode recording and imaging. Each sample was used for a maximum of 3 h.

Oxygen Reduction and Antioxidant Preparation. OxyFluor (OF-0005, Oxyrase) was added to SL-15 containing dye at 3 units/ml (43), and nitrogen gas was perfused over the dish, resulting in an oxygen concentration reduction in the medium from $\approx$21% to 0.0% after 5 min. The OxyFluor did not perturb the electrophysiological parameters of the neurons during the tens of minutes of experiment time; resting Vm and AP properties were the same with and without OxyFluor.

Astaxanthin (A9335, Sigma) was used as a free radical scavenger (44, 45). The carotenoid loading procedure developed by Cooney *et al.* (46) did not work for Astaxanthin in SL-15 medium, likely because of the high-salt concentration of SL-15. Therefore, we developed a protocol where Astaxanthin was dissolved in a solution of 20% Pluronic in DMSO (P-3000, Molecular Probes) at a concentration of 20 mM. Fifty microliters of this solution was added to 2 ml of SL-15 containing dye with vortexing and then filtered through a 0.22-μm filter. The neurons were then incubated in this solution for 30 min.

Following the observations of Hirase *et al.* (18), Trolox (238813, Sigma), a soluble form of vitamin E, was also tested. This antioxidant was easily dissolved in SL-15 containing dye at a concentration of 1 mM.

Analysis. The electrophysiology records were analyzed by using ORIGIN 6.0 (Microcal Software, Northampton, MA). Traces containing spontaneous APs and/or large discontinuities not associated with physiological events were discarded. Errors are given in standard errors. $1/(\mathrm{SE})^2$ weighing was used during the fit procedure. The errors obtained from the fit procedures were scaled with reduced χ^2. The goodness of fit parameter R^2 was used to validate linear fits. The optical records were analyzed by software written in LABVIEW 6.1 (National Instruments, Austin, TX). A Vm-independent bleaching effect during line scanning was corrected from the recordings by fitting the signal baseline with a biexponential function.

We thank W. Zipfel and R. Williams for instrumentation support and helpful discussions and M. Williams and F. Vanzi for discussions and reading of this manuscript. L.S. thanks Cornell University for his visit and was supported by European Laboratory for Nonlinear Spectroscopy Grant MTKD-CT-2004-509761. D.A.D. and W.W.W. were supported by National Institutes of Health Grants P41 EB001976-1716, GM08267, and GM07469.

1. Zochowski, M., Wachowiak, M., Falk, C. X., Cohen, L. B., Lam, Y. W., Antic, S. & Zecevic, D. (2000) *Biol. Bull.* **198,** 1–21.
2. Salzberg, B. M., Davila, H. V. & Cohen, L. B. (1973) *Nature* **246,** 508–509.
3. Salzberg, B. M., Grinvald, A., Cohen, L. B., Davila, H. V. & Ross, W. N. (1977) *J. Neurophysiol.* **40,** 1281–1291.
4. Grinvald, A. & Hildesheim, R. (2004) *Nat. Rev. Neurosci.* **5,** 874–885.
5. Briggman, K. L., Abarbanel, H. D. & Kristan, W. B., Jr. (2005) *Science* **307,** 896–901.
6. Dombeck, D. A., Blanchard-Desce, M. & Webb, W. W. (2004) *J. Neurosci.* **24,** 999–1003.
7. Dombeck, D. A., Sacconi, L., Blanchard-Desce, M. & Webb, W. W. (2005) *J. Neurophysiol.* **94,** 3628–3636.
8. Moreaux, L., Sandre, O., Charpak, S., Blanchard-Desce, M. & Mertz, J. (2001) *Biophys. J.* **80,** 1568–1574.
9. Bouevitch, O., Lewis, A., Pinevsky, I., Wuskell, J. P. & Loew, L. M. (1993) *Biophys. J.* **65,** 672–679.
10. Bullen, A. & Saggau, P. (1999) *Biophys. J.* **76,** 2272–2287.
11. Moreaux, L., Pons, T., Dambrin, V., Blanchard-Desce, M. & Mertz, J. (2003) *Opt. Lett.* **28,** 625–627.
12. Pons, T., Moreaux, L., Mongin, O., Blanchard-Desce, M. & Mertz, J. (2003) *J. Biomed. Opt.* **8,** 428–431.
13. Denk, W., Strickler, J. H. & Webb, W. W. (1990) *Science* **248,** 73–76.
14. Zipfel, W. R., Williams, R. M. & Webb, W. W. (2003) *Nat. Biotechnol.* **21,** 1369–1377.
15. Helmchen, F. & Denk, W. (2005) *Nat. Methods* **2,** 932–940.
16. Parsons, T. D., Salzberg, B. M., Obaid, A. L., Raccuia-Behling, F. & Kleinfeld, D. (1991) *J. Neurophysiol.* **66,** 316–333.
17. Obaid, A. L., Koyano, T., Lindstrom, J., Sakai, T. & Salzberg, B. M. (1999) *J. Neurosci.* **19,** 3073–3093.
18. Hirase, H., Nikolenko, V., Goldberg, J. H. & Yuste, R. (2002) *J. Neurobiol.* **51,** 237–247.
19. Boulatov, R., Collman, J. P., Shiryaeva, I. M. & Sunderland, C. J. (2002) *J. Am. Chem. Soc.* **124,** 11923–11935.
20. Schroeder, W. A. & Johnson, E. A. (1995) *J. Biol. Chem.* **270,** 18374–18379.
21. Palozza, P. & Krinsky, N. I. (1992) *Arch. Biochem. Biophys.* **297,** 291–295.
22. Moreaux, L., Sandre, O. & Mertz, J. (2000) *J. Opt. Soc. Am. B* **17,** 1685–1694.
23. Antic, S. D. (2003) *J. Physiol. (London)* **550,** 35–50.
24. Rall, W. & Rinzel, J. (1973) *Biophys. J.* **13,** 648–687.
25. Rinzel, J. & Rall, W. (1974) *Biophys. J.* **14,** 759–790.
26. Campagnola, P. J., Millard, A. C., Terasaki, M., Hoppe, P. E., Malone, C. J. & Mohler, W. A. (2002) *Biophys. J.* **82,** 493–508.
27. Zipfel, W. R., Williams, R. M., Christie, R., Nikitin, A. Y., Hyman, B. T. & Webb, W. W. (2003) *Proc. Natl. Acad. Sci. USA* **100,** 7075–7080.
28. Dombeck, D. A., Kasischke, K. A., Vishwasrao, H. D., Ingelsson, M., Hyman, B. T. & Webb, W. W. (2003) *Proc. Natl. Acad. Sci. USA* **100,** 7081–7086.
29. Brown, E., McKee, T., diTomaso, E., Pluen, A., Seed, B., Boucher, Y. & Jain, R. K. (2003) *Nat. Med.* **9,** 796–800.
30. Williams, R. M., Zipfel, W. R. & Webb, W. W. (2005) *Biophys. J.* **88,** 1377–1386.
31. Konig, K., Becker, T. W., Fischer, P., Riemann, I. & Halbhuber, K. J. (1999) *Opt. Lett.* **24,** 113–115.
32. Konig, K., Liang, H., Berns, M. W. & Tromberg, B. J. (1996) *Opt. Lett.* **21,** 1090–1092.
33. Konig, K., So, P. T. C., Mantulin, W. W. & Gratton, E. (1997) *Opt. Lett.* **22,** 135–136.
34. Koester, H. J., Baur, D., Uhl, R. & Hell, S. W. (1999) *Biophys. J.* **77,** 2226–2236.
35. Hopt, A. & Neher, E. (2001) *Biophys. J.* **80,** 2029–2036.
36. Patterson, G. H. & Piston, D. W. (2000) *Biophys. J.* **78,** 2159–2162.
37. Chen, T. S., Zeng, S. Q., Luo, Q. M., Zhang, Z. H. & Zhou, W. (2002) *Biochem. Biophys. Res. Commun.* **291,** 1272–1275.
38. Chirico, G., Cannone, F., Baldini, G. & Diaspro, A. (2003) *Biophys. J.* **84,** 588–598.
39. Shear, J. B., Xu, C. & Webb, W. W. (1997) *Photochem. Photobiol.* **65,** 931–936.
40. Mertz, J. (1998) *Eur. Phys. J. D* **3,** 53–66.
41. Neuman, K. C., Chadd, E. H., Liou, G. F., Bergman, K. & Block, S. M. (1999) *Biophys. J.* **77,** 2856–2863.
42. Goldberg, D. & Schacher, S. (1998) in *Culturing Nerve Cells*, eds. Banker, G. & Goslin, K. (MIT Press, Cambridge, MA), pp. 213–236.
43. Waterman-Storer, C. M., Sanger, J. W. & Sanger, J. M. (1993) *Cell Motil. Cytoskeleton* **26,** 19–39.
44. Gonzalez, J. E. & Tsien, R. Y. (1997) *Chem. Biol.* **4,** 269–277.
45. Cogdell, R. J. & Frank, H. A. (1987) *Biochim. Biophys. Acta.* **895,** 63–79.
46. Cooney, R. V., Kappock, T. J. T., Pung, A. & Bertram, J. S. (1993) *Methods Enzymol.* **214,** 55–68.